JOURNAL OF MATERIALS SCIENCE 28 (1993) 4944–4956

Deformation and failure of adhesive bonds under shear loading

H. CHAI*
National Institute of Standards and Technology, Polymers Division, Gaithersburg, MD 20899, USA

Experiments have shown that certain mechanical properties can be greatly enhanced when a material is stressed while under tight spatial constraint. In this work, the post-yield behaviour of brittle and ductile epoxy resins used as thin adhesive bonds was determined using the "napkin ring" shear test. Real-time observations of the deformation in the bond as well as SEM post-failure analysis were employed to gain information on the failure process. The complete stress–strain histories of the adhesives were established for bond thicknesses ranging from the micrometre level up to values large enough to expose the bulk properties. The most dramatic variations occurred for the ultimate shear strain, γ_f; for the brittle adhesive, γ_f increased by over 30-fold relative to the bulk material when the bond thickness, t, was decreased to a few micrometres. Experimental evidence and analytical considerations suggest that the decline of γ_f with t was due to premature bond failure caused by tensile microcracks or voids that were formed in the interlayer during loading, with the specific γ_f versus t relationship being a mere reflection of the variations in the degree of stress concentration at the tip of the flaws. The astonishingly large value of γ_f (i.e. 2.8–3.4)found for the brittle epoxy in the micrometre thickness range, is believed to represent the intrinsic shear strain of this material.

1. Introduction

The joining of two distinct materials by a third phase is a practice of long-standing interest in a variety of industrial and technological applications, including traditional adhesive bonding, brazing, soldering, welding and composite materials. More recently, microlamination concepts have emerged where thin layers of differing materials are joined to form a microlaminate whose mechanical properties are superior to those of the individual components. For example, the ultimate tensile strain of a microlaminate made from alternating layers of brittle and ductile polymers was found to increase by over 15-fold upon decreasing the layer thickness from 25 μm to 1.5 μm [1]. Similar effects were also found in metal-based (Al–Cu) microlaminates prepared by vapour deposition; for layer thicknesses $\leqslant$ 70 nm, the laminate yield stress was over four times larger and the laminate ultimate tensile stress approximately three times larger than the values predicted by the rule of mixtures for the aluminium and copper [2]. The cause of such improvements is understood only qualitatively, however, being attributed to suppression of crazing or cracking in the brittle layer [1] or impedance of dislocation generation [2]. Unfortunately, because the laminate performance is evaluated from overall laminate response, the specific contribution of each material phase is not easily isolated. It is the purpose of this work to study the behaviour of each material phase separately and under well-controlled, unambiguous and simplified test conditions so as to facilitate a rational approach to optimal design.

This work was originally motivated by recent Mode II fracture tests on adhesively bonded joints [3]. The results show that the adhesive fracture energy is greatly affected by the bond thickness, t. In particular, for an unmodified epoxy resin, several-fold variation in t led to as much as a 35-fold increase in the fracture energy, G_{IIC}. Because the latter is directly related to the deformation capability of the adhesive, it was felt that the key to understanding such dramatic toughness variations lies in understanding the effect of bond thickness on the post-yield behaviour of the unflawed adhesive. The "napkin ring" shear test (see Fig. 1), originally proposed by de Bruyne [4], seems ideally suited for this purpose. This specimen is composed of two tubular adherends butted coaxially to the adhesive to be studied. Loading is applied by a remote torque. By making the bond sufficiently narrow, radial variations are minimized. This leads to a state of simple pure shear stress within the interlayer. Other test specimens that have been extensively used for the intended purpose of measuring adhesive shear properties include the well known lap–shear, pin and collar (e.g. [5, 6]), stiff-adherend [7, 8] and the Chisholm–Jones shear specimen [9]. The main drawbacks of these tests are that the shear stress and shear strain vary along the glue line, and that some tensile

* *Present address*: Department of Mechanics, Materials and Structures, Tel-Aviv University, Tel-Aviv, Israel.

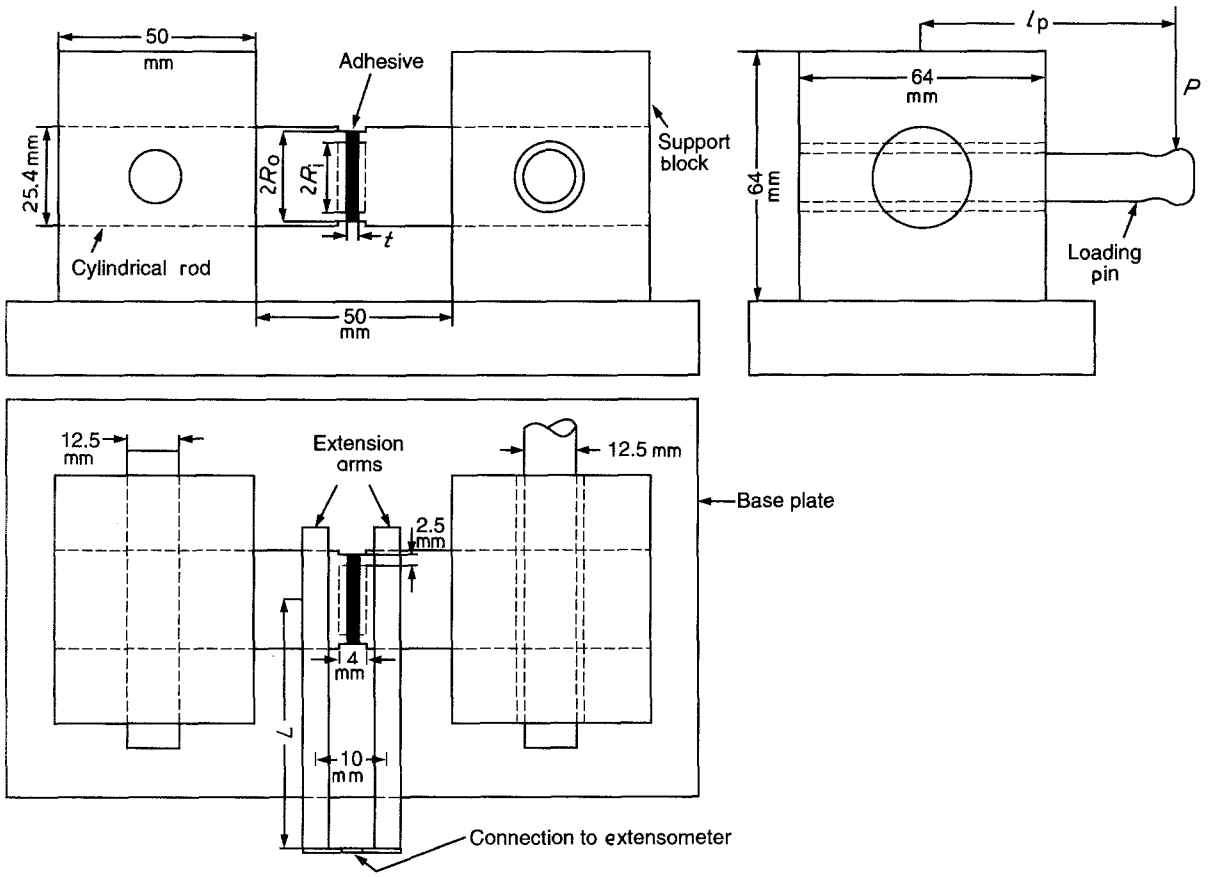

Figure 1 Schematic drawing of the napkin ring shear specimen. P is the applied axial load and l_p is the distance between the load line and the specimen axis.

stresses are produced at the bond terminus. While these effects can be greatly reduced by a proper design (e.g. using a 90° opening angle at the bond terminus [7, 8]), the napkin ring specimen was adopted in this work because, as will be seen later, it affords a rather straightforward means to measure accurately the shear strain for extremely thin bonds.

The effect of bond thickness on adhesive shear strength was reported by a number of investigators [5, 6, 10–13], the majority of which were concerned with adhesive bonding applications that call for relatively thick bonds (typically > 0.1 mm). It was generally found that the failure stress, τ_f, tends to increase somewhat with decreasing t, although no adequate explanation for this effect was provided. Another adhesive property of interest is the ultimate shear strain, γ_f; the unique significance of this to the structural integrity of adhesive bonds apparently was first recognized by Hart-Smith [14]. Despite this, the only systematic study of the effect of bond thickness on γ_f known to this author is due to Stringer [10], who has generated data for a number of ductile adhesives, either filled or unfilled, over the range $0.1 \text{ mm} < t < 1 \text{ mm}$. It is noted that because in the butt joints employed in [10] the adhesive bond occupied the entire rod diameter, the stress and strain in the adhesive vary along the radial direction. This raises concern about the significance of the measured ultimate shear strain. A number of investigators have provided stress–strain curves from which γ_f can be extracted. The bond thickness used ranged from 100–200 μm. The reported values of γ_f for ductile adhesives, either supported or unsupported, range from 40%–200% (7, 8, 10, 14–17]. The data for brittle adhesives are more scarce, and the nominal values reported are in the range of 10%–20% [11, 14, 15, 17].

In this work, the deformation history of the adhesive interlayer was established for brittle and toughened epoxy systems currently used in composite materials. In order to be able to address applications to composites and microlaminates, the bond thickness studied included the micrometre range. This is in addition to the sub-millimetre range relevant to traditional adhesive bonding applications.

2. Experimental procedure

2.1. Apparatus

Details of the test specimen and loading are given in Fig. 1 together with relevant dimensions. As shown, a special fixture was designed to convert the applied axial load, P, into torsional displacement at the bond region. The specimen was made of two cylindrical rods which were machined at their edges to a ring shape. The depth of the ring was 2 mm while the bond width (i.e. the difference between the outer and inner radii of the bond, R_o and R_i, respectively) was 2.5 mm. Each of the rods is supported by a hollow prismatic aluminium block. To minimize bending stresses, the clearance between the surface of the rods and the inner bore of the blocks was kept below 50 μm. The supporting blocks were firmly bolted to a base plate made of steel. The latter was fixed to the frame of the testing

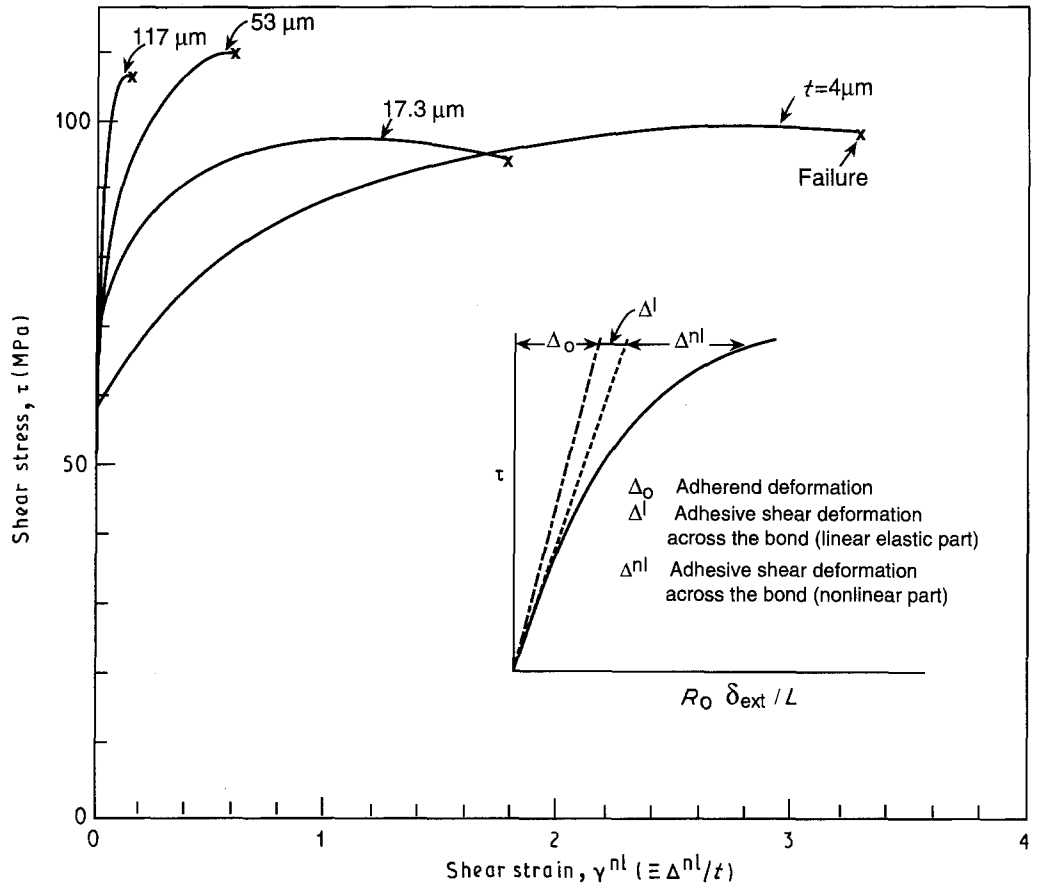

Figure 2 Stress–strain curves for four representative bond thicknesses. Adhesive is Narmco 5208, adherend is 5086 Al alloy. γ^{nl} is the non-linear part of adhesive shear strain, given by Δ^{nl}/t. The insert shows a typical stress–displacement record; δ_{ext} is the extensometer output.

machine. One cylindrical rod was fixed to its supporting block by means of a 12.5 mm diameter steel pin while the other was free to rotate. Circumferential deformations in the rods were induced by applying axial load to a steel pin which was inserted into the right-hand side rod. To facilitate free rotation, the hole in the supporting block which accommodated the loading pin was made larger than the pin diameter. This clearance also allowed for a free axial movement of the rods, which ensured that no axial stress may set up in the bond during adhesive deformation. To minimize friction, all moving parts were oiled; loading–unloading curves in the linearly elastic regime of the adhesive virtually overlapped.

As shown in Fig. 1, a standard extensometer (MTS*) was used to record the relative shearing displacement across the bond. The extensometer was attached to the ends of two long extension arms which were firmly connected to the cylindrical rods, one on each side of the bond. As shown in the insert in Fig. 2, the extensometer output consisted of contributions from both the adhesive and adherends (i.e. the total deformation between the two extension arms), and it was not possible to separate the two with any degree of accuracy, particularly for thin bonds. However, we were primarily interested here in the non-linear part of the adhesive deformation across the bond, Δ^{nl}, which can be easily determined by subtracting from the total output ($\Delta_o + \Delta^l + \Delta^{nl}$), the output corresponding to a straight line tangential to the initial slope of the stress–strain curve (i.e. the dashed line in Fig. 2). Thus

$$\gamma^{nl} \equiv \frac{\Delta^{nl}}{t} = \frac{\delta^{nl}_{ext} R_o}{Lt} \quad (1)$$

where δ^{nl}_{ext} is the non-linear part of extensometer output, γ^{nl} the non-linear part of adhesive shear strain, and L the length of extension arms. In the following, results will be presented only for γ^{nl}; the total adhesive shear strain, γ_t, can be found from

$$\gamma_t = \gamma^{nl} + \frac{\tau}{G} \quad (2)$$

where τ and G are the adhesive shear stress and shear modulus, respectively. Note G may vary with bond thickness.

2.2. Materials

Two amorphous adhesives were evaluated, namely Narmco 5208 (Whittaker Co.) and BP-907 (American Cyanamid Co.). The first is a highly cross-linked, brittle epoxy with approximately 2% ultimate tensile strain and a G_{IC} value of 73 $N\,m^{-1}$ [18] while BP-907

* Certain commercial materials and equipment are identified in this paper in order to specify adequately the experimental procedure. In no case does such identification imply recommendation or endorsement by the National Institute of Standards and Technology (NIST) nor does it imply necessarily the best available for the purpose.

is an epoxy resin toughened by proprietary additives. This material exhibits a mild degree of ductility, with 5% ultimate tensile strain [18] and a G_{IC} value of 500 $N m^{-1}$ [3]. Note that Narmco 5208 is virtually identical to the H3502 adhesive used in a previous work [3]. An extensive study of the effect of bond thickness on the fracture energy for these adhesives is given elsewhere [3, 18]. The adherends were either 7075 Al alloy (BP-907) or 5086 Al alloy (Narmco 5208 and BP-907); the detailed usage is specified along with the data. The 7075 Al alloy was initially used for both polymers, but it led to adhesive failure when testing Narmco 5208 at all values of t and when testing BP-907 at extremely small values of t. It was found that the 5086 Al alloy, which was purer and less amenable to oxidation following specimen cleaning, gave rise to cohesive failure for both adhesives.

2.3. Bond surface preparation

The bonding surfaces were polished with successively finer grit metallographic papers down to a sub-micrometre surface roughness finish. The adherends were cleaned as follows: degrease in a bath of trichloroethylene for 30 min, immerse in MEK solvent for 30 min, chemically etch in a bath of sodium dichromate/sulphuric acid/distilled water (3/10/30 weight ratio) at 70 °C, wash, and dry.

2.4. Bonding

The adhesives were debulked and degassed in vacuum for 30 min, while at 121 °C. After applying the molten adhesives to the bonding surfaces, the two specimen halves were laid on a specially constructed wedge to ensure good alignment. To facilitate good contact between the adhesive and adherends, a small axial compression force was applied to the flat ends of the cylindrical rods via a specially designed C-clamp tool. The bond thickness was controlled by inserting copper wires or glass fibres of the desired thickness at three locations within the bond. For bonds a few micrometres thick, no spacers were used. Instead, the thickness was controlled by the axial force applied to the specimen ends. For yet thinner bonds, a press machine was used, with the bond thickness being set, through trial and error, by the level of compression load, applied along the axis of the rods.

The specimens were cured in an air-circulation oven in accordance with the manufacturer's recommended curing cycle: BP-907, heat to 121 °C and hold for 1 h, increase temperature to 180 °C over a 30 min period, hold for 1 h, and slowly cool to RT; Narmco 5208, as above, except the curing time at 180 °C was 2 h. Also, this material was post-cured at 204 °C for 4 h.

After curing, the bonded specimens were milled in the area of the bond to a depth of 0.3 mm and a width of 4 mm so as to produce the final ring configuration shown in Fig. 1. This operation was undertaken because of a concern that the bonding surfaces near the outer edge of the bond may deviate from flatness. The milled surface was then polished with a strip of fine grit metallographic paper, and the bond thickness measured with the aid of an optical microscope at four locations around the bond.

2.5. Video recording

For some tests, the adhesive deformation was observed using a video camera. The latter was attached to a stereo optical microscope, which provided magnification up to $\times 140$. The observed bond region was coated with a diluted typewriter correction fluid. To facilitate quantitative determination of adhesive shear strain, an array of line marks paralleling the longitudinal axis of the specimen was manually scribed on the outer surface of the bond using a sharp razor blade; the slope of the deformed lines provided the total engineering shear strain. With this technique, good resolution of shear strains was achieved for bond thicknesses greater than 25 μm.

2.6. Testing

Torsion tests were carried out on a MTS Servohydraulic testing machine operated in a stroke-controlled mode. The specimens were loaded to complete failure, and the load versus extensometer displacement recorded on a chart recorder. Although the loading was stroke controlled, because of the relatively large strain energy stored outside the bond region, the actual loading was more "fixed load" type than the intended "fixed grip", particularly so for very thin bonds (e.g. for a 2.5 μm thick bond, the circumferential displacement absorbed in the adherends may exceed 50 times that of the adhesive). As a result, the actual strain rate of the adhesive, γ, varied during the deformation, typically increasing with increasing the slope of the stress–strain curve. To facilitate determination of $\dot{\gamma}$, the evolving stress–strain curve was marked at specific time intervals; division of the adhesive differential strain by the elapsed time gave the instantaneous strain rate.

The adhesive shear stress was determined from the following equilibrium condition

$$\begin{aligned} T &= Pl_p \\ &= 2\pi \int_{R_i}^{R_o} \tau r^2 dr \\ &= \frac{2\pi\tau(R_o^3 - R_i^3)}{3} \end{aligned} \tag{3}$$

or

$$\tau = \frac{1.5Pl_p}{\pi(R_o^3 - R_i^3)} \tag{4}$$

where P, T and l_p are the applied load, the resulting torque and the distance between the load line and the longitudinal axis of the specimen, respectively. Over 200 test samples were manufactured. Many were rejected because of misalignment, non-uniformity of bond thickness and joint starvation. Only good-quality specimens with less than 10% bond thickness variations were tested. Of these, some failed prematurely (i.e. sometimes well before adhesive yielding

took place). Some of the specimens with extremely thin bonds failed upon securing them to their fixture, apparently because of unavoidable specimen bending which produced large tensile stresses in the bond. Of the specimens manufactured, only 19 samples for BP-907 and 16 for Narmco 5208 resulted in what is believed to be valid data for ultimate strain and ultimate stress.

3. Results

3.1. Brittle epoxy (Narmco 5208)

Stress–strain curves for a number of representative bond thicknesses are shown in Fig. 2. The strain was determined from the extensometer output and Equation 1. As mentioned earlier, only the non-linear part of the adhesive deformation is given. Common to all bond thicknesses is an initial linearly elastic response (not shown) which is followed by a non-linear behaviour up to final failure. The dependence of failure stress, τ_f on t is shown in Fig. 3 for both the 7075 and 5086 Al adherends. The adhesive strain rate, $\dot{\gamma}^{nl}$, at final failure was approximately 0.003 s^{-1}. The joint strength obtained with the 7075 alloy appears slightly greater than that for the 5086 alloy, but the difference is within experimental scatter. The failure stress seems quite independent of t. This is except for very thin bonds ($t < 10$ μm), where τ_f seems to decrease as t is decreased, but the specific relationship is obscured by a relatively large experimental scatter.

The dependence of ultimate adhesive shear displacement (non-linear part), Δ_f^{nl}, and ultimate adhesive shear strain, γ_f^{nl}, on bond thickness is shown in Fig. 4; the curve for γ_f^{nl} was obtained by dividing values from the fitting curve for Δ_f^{nl} by t. For relatively thick bonds ($t > 75$ μm), the failure strain tends to approach a plateau, the nominal value (several per cent) of which is similar to values reported for other brittle epoxies [11, 14, 15, 17] evaluated at comparable bond thicknesses. For $t < 75$ μm, γ_f^{nl} increases with decreasing t, first moderately but later sharply, reaching a value as large as 340% at $t = 9$ μm. Thereafter, γ_f^{nl} exhibits a slight reversal in trends, the extrapolated value at zero bond thickness is 240%.

3.2. Toughened epoxy (BP-907)

Representative stress–strain curves for this material are given in Fig. 5. As shown, while the data for relatively thick bonds (Fig. 5a) were generated using the 7075 Al adherend, those of the very thin bonds (Fig. 5b) were carried out using the 5086 Al alloy. Comparative tests showed that the enhanced adhesion quality of the 5086 alloy became apparent only for $t < 5$–10 μm, where the criticality of the metal/matrix interface is apparently accentuated. The initial response of this toughened epoxy at relatively large values of t (Fig. 5a) is nearly elastic–perfectly plastic. However, as the strain is increased, additional phases of either strain softening (Fig. 5a, $t = 0.63$ mm) or

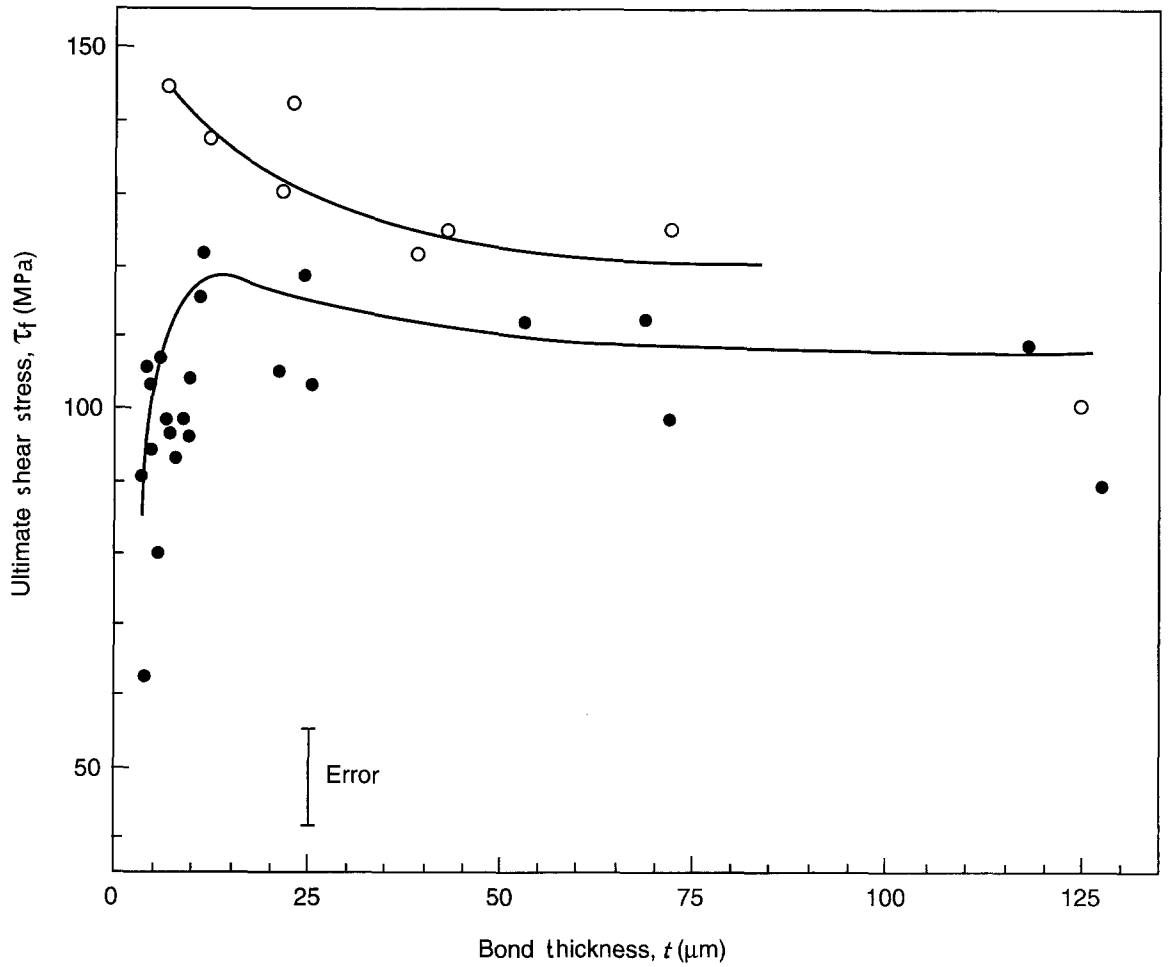

Figure 3 Shear stress at failure as a function of bond thickness for Narmco 5208. Adherend: (●) 5086 Al alloy, (○) 7075 Al alloy.

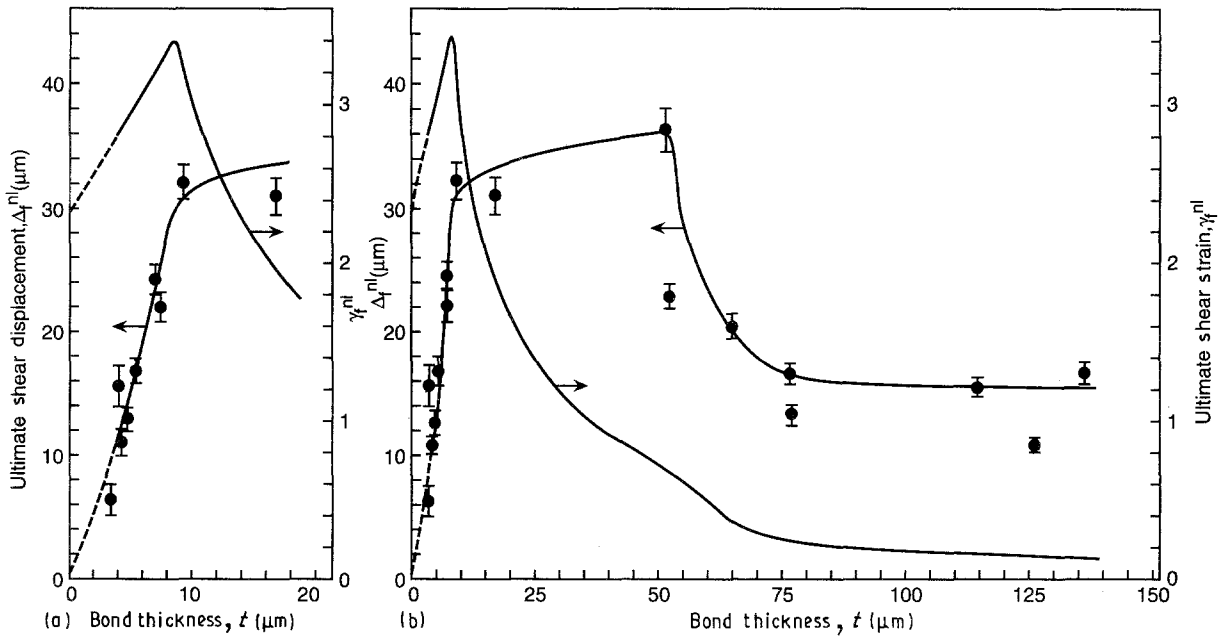

Figure 4 (a) An enlargement of the thin-bond region in (b). (b) Ultimate shear displacement (non-linear part) across the bond, Δ_f^{nl}, and ultimate shear strain, γ_f^{nl}($\equiv \Delta_f^{nl}/t$) as a function of bond thickness. The curve for γ_f^{nl} was generated from the fitted curve for Δ_f^{nl}. (- - -) Extrapolations of the test data to the origin. Adhesive is Narmco 5208, adherend is 5086 Al alloy.

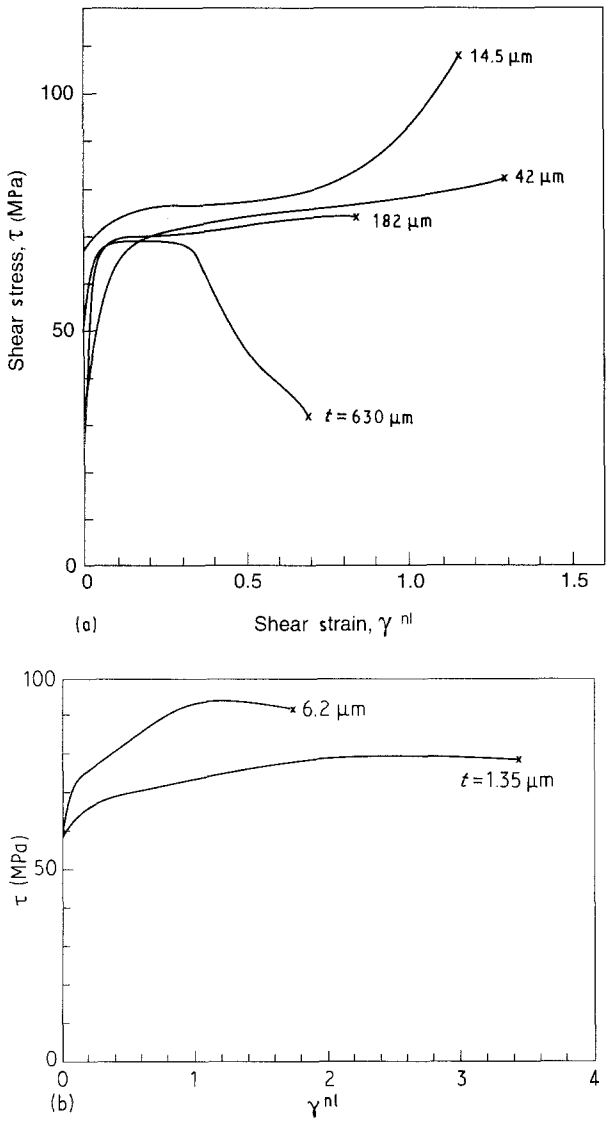

Figure 5 Stress–strain curves for a number of representative bond thicknesses. Adhesive is BP-907, adherend is (a) 7075 Al alloy or (b) 5086 Al alloy.

strain hardening (Fig. 5a, $t = 14.5$ μm) occur, the particular mode of which depended on bond thickness. For very thin bonds (Fig. 5b), the phase of strain hardening is seen to be followed by yet another phase of common yielding. The second phase of yielding, which contributes greatly to the ultimate strain, was not encountered when using the 7075 alloy as the adherend, probably because of insufficient adhesion. The actual strain rate in the adhesive was evaluated as discussed in Section 2.6. The results for the yield segment of the stress–strain curve can be described reasonably well as follows

$$\dot{\gamma}^{nl} = 0.025 \times (1 - 7.5t\,(\text{mm}))\text{s}^{-1} \quad t < 0.125\,\text{mm} \quad (5a)$$

$$\dot{\gamma}^{nl} = 0.0015\text{s}^{-1} \quad t > 0.125\,\text{mm} \quad (5b)$$

For bonds which exhibited strain hardening, the strain rate just before failure was determined to be approximately 0.006 s^{-1}, irrespective of t.

The dependence of yield stress (taken as the stress at the flat portion of the stress–strain curve) and failure stress on t is shown in Fig. 6. While the yield stress seems independent of t, the failure stress exhibits a complex behaviour; for $t > 0.1$ mm, τ_f decreases with t while the opposite holds for $t < 40$ μm. τ_f attains a maximum at $t = 14$ μm, its nominal value exceeds by over 40% the yield stress. Similarly to the brittle epoxy, τ_f seems to decline when t becomes very small (< 14 μm).

The variations of ultimate shear displacement across the bond and ultimate shear strain with bond thickness are shown in Fig. 7. γ_f^{nl} seems to approach a plateau when t is increased beyond 0.34 mm. The corresponding value (70%) considerably exceeds that obtained for the same adhesive and same bond thickness using the lap–shear specimen (40% [15]). It is

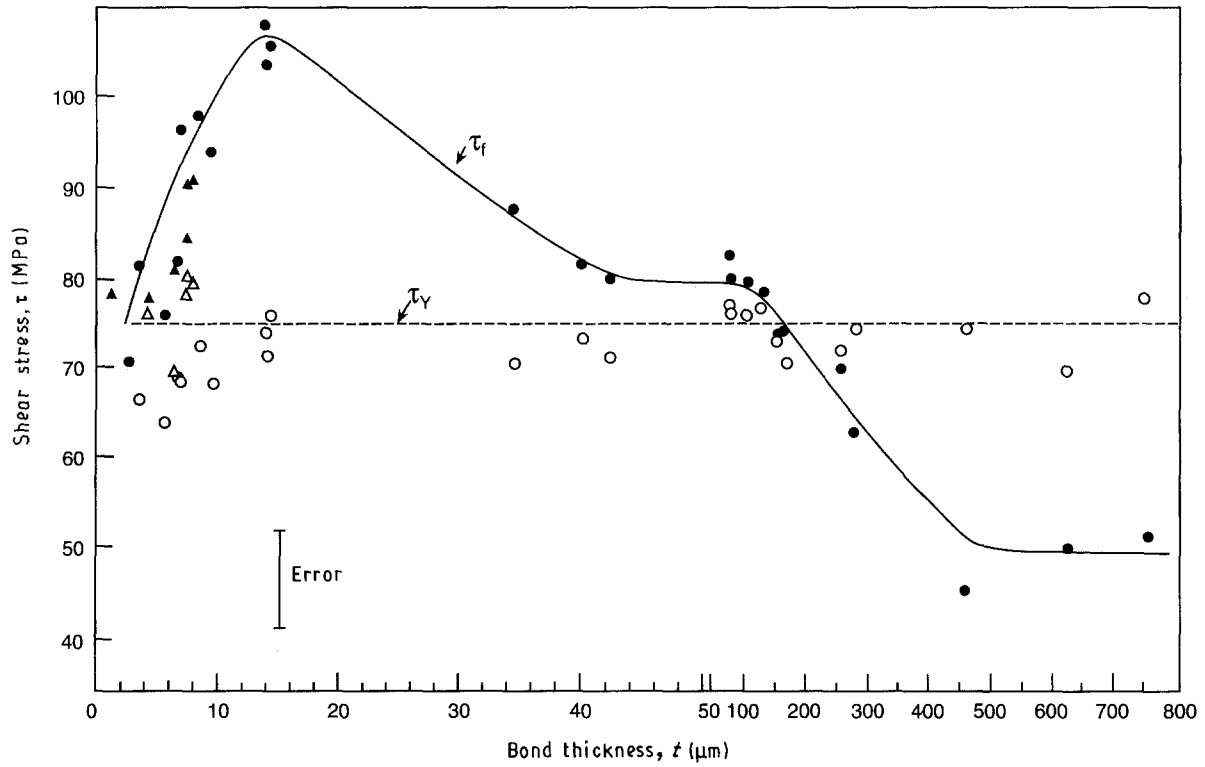

Figure 6 (●, ▲) Failure stress and (○, △) yield stress as a function of bond thickness for (○, ●) 7075 Al alloy and (△, ▲) 5086 Al alloy. Adhesive is BP-907.

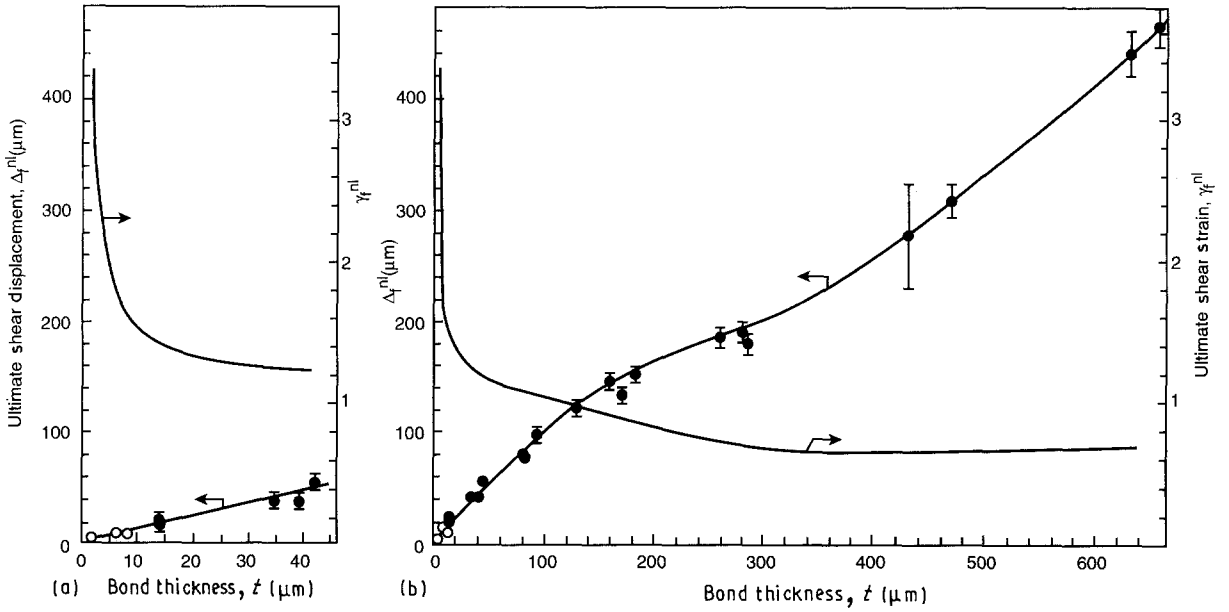

Figure 7 (a) An enlargement of the thin-bond region in (b). (b) Ultimate shear displacement across the bond and ultimate shear strain as a function of bond thickness for (●) 7075 Al alloy, (○) 5086 Al alloy. Adhesive is BP-907.

possible that the reduced value in [15] is due to a premature failure caused by tensile stresses at the bond terminus. Similarly to the brittle epoxy, γ_f^{nl} exhibits a steep rise when the bond thickness becomes very small (< 10 μm), reaching a value as large as 340% at $t = 1.35$ μm. Unfortunately, the precise behaviour in the micrometre thickness range is not very well established due to the scarcity of the data. Repeated attempts (five) to generate data in the range $t < 5$ μm were unsuccessful because of recurrence of premature joint failure. Such failure may be attributed to the development of tensile stresses in the bond which are as a result of bending specimen and/or the prevalent "fixed load" condition which tend to promote catastrophic failure. Apparently, a more sophisticated testing approach is needed to establish the material behaviour for very thin bonds.

Because the behaviour of γ_f^{nl} for $t < 5$ μm was assessed based on a single datum point ($t = 1.35$ μm), concern arose as to the accuracy of that segment of the curve. As indicated earlier, in extracting γ_f^{nl} from the extensometer output, the assumption was made that the deformation of the adherends is linearly elastic. However, because of the smallness of the deformations

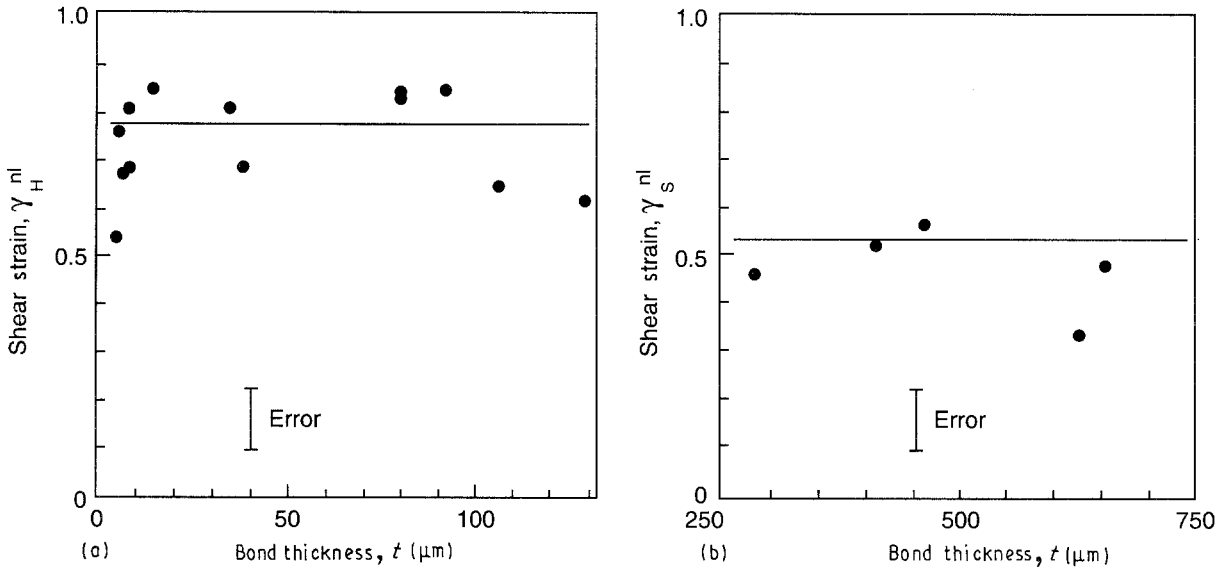

Figure 8 (a) Shear strain at initiation of strain hardening, γ_H^{nl}, and (b) shear strain at initiation of strain softening, γ_S^{nl}, as a function of bond thickness. Adhesive is BP-907.

involved, even small plastic deformations in the adherends may greatly affect the calculated γ_f^{nl}. An estimate of the former was made by examining the load versus extensometer output for very thin bonds. It was concluded that the non-linear displacement in the adherends in the region contained by the two extensometer arms must be less than 0.75 μm. Subtracting this value from Δ_f^{nl} (= 5.3 μm), one finds $\gamma_f^{nl} = 2.83$. This is 20% less than the value depicted in Fig. 7.

Fig. 6 shows that strain hardening and strain softening occurs for small and large bond thicknesses, respectively; the transition seems to take place at $t = 0.04 - 0.1$ mm. For a given value of t within each of these phases, the incipient strain for hardening or softening can be easily determined from the stress–strain curves. The results given in Fig. 8, show that irrespective of t, hardening occurs once γ^{nl} exceeds 77% (Fig. 8a) while softening takes place when γ^{nl} exceeds 52% (Fig. 8b).

Fig. 9 shows a sequence of video records which provide information on the evolution of damage and deformations during loading as they appear on the outer surface of the bond. As indicated earlier, the distinct dark lines traversing the bond are pre-produced scratch marks. As shown, during the entire deformation history the shear strain is quite homogeneous (uniform across the bond). This is except around voids, where local perturbations in the strain field can be seen. The first large void to appear in the observed region is identified by point A; the corresponding shear strain in the bond is 51% of the failure strain. (Note: the large dark spot seen above point A is an artefact, not a void.) Although no visible voids were observed in prior frames, it is likely that smaller voids unresolved by the camera were formed at earlier stages. At 85% ultimate shear strain (Fig. 9b), the void at point A is considerably larger. Also, an additional large void (point B) appeared approximately three bond thicknesses away. Immediately prior to failure (Fig. 9c), an additional large void appeared (point C). Final failure occurred by rapid debonding along the right-hand side of the interface, as can be seen from the discontinuity of the scratch marks along that interface.

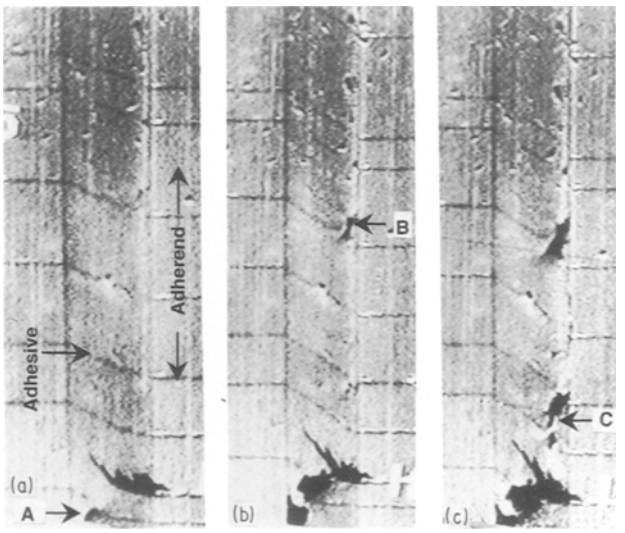

Figure 9 A sequence of video records showing the evolution of deformation and damage in the adhesive (BP-907) during loading, $t = 0.285$ mm. (a) $\gamma^{nl}/\gamma_f^{nl} = 0.51$, (b) $\gamma^{nl}/\gamma_f^{nl} = 0.85$, (c) $\gamma^{nl}/\gamma_f^{nl} = 1.0$. The dark lines traversing the bond are pre-produced scratch marks. Final failure immediately followed the frame in (c), and it occurred by debonding near the right-hand side of the metal/adhesive interface. Note that the dark spot appearing above point A in (a) is an artefact, not a void.

3.3. SEM analysis

3.3.1. Brittle epoxy (Narmco 5208)

Figs 10 and 11 exemplify, respectively, the morphology for the bond thickness range where Δ_f^{nl} is nearly constant (10 μm $< t <$ 60 μm) or γ_f^{nl} decreases sharply with t, and for thick bonds where γ_f^{nl} tends to approach a plateau. In both cases, the failure surface is characterized by a consistent array of microcracks which extend in the radial direction and which spatial frequency is several times the bond thickness. Final

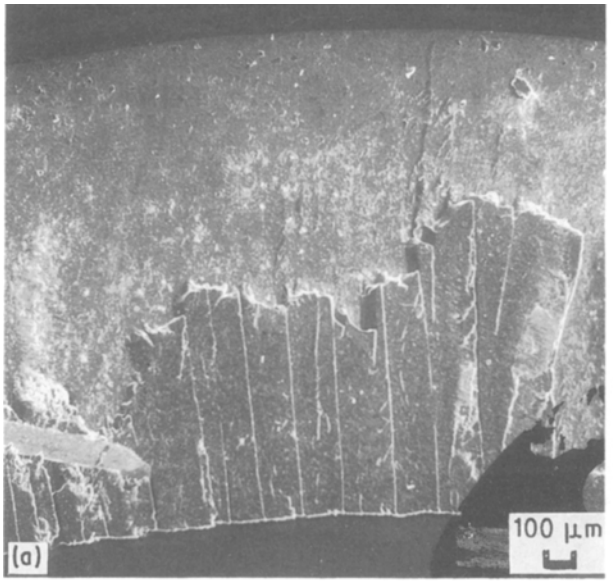

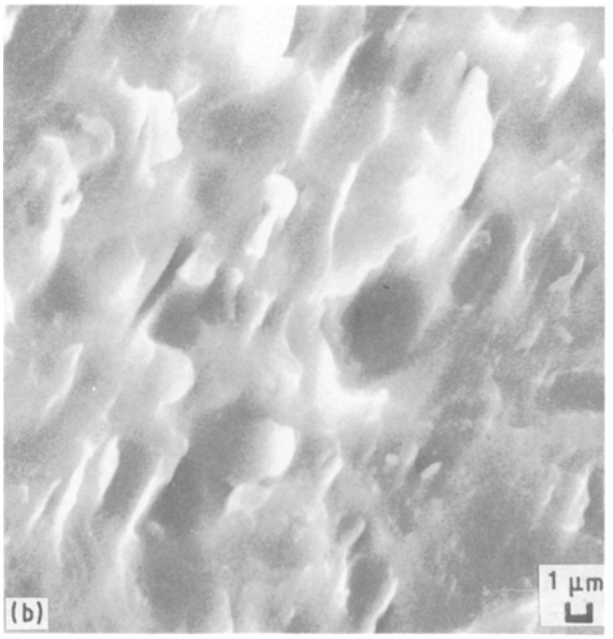

Figure 10 (a, b) Scanning electron micrographs for Narmco 5208 showing the failed bond at two magnifications, $t = 53$ µm. The sequence of white lines extending in the radial direction are microcracks extending across the bond.

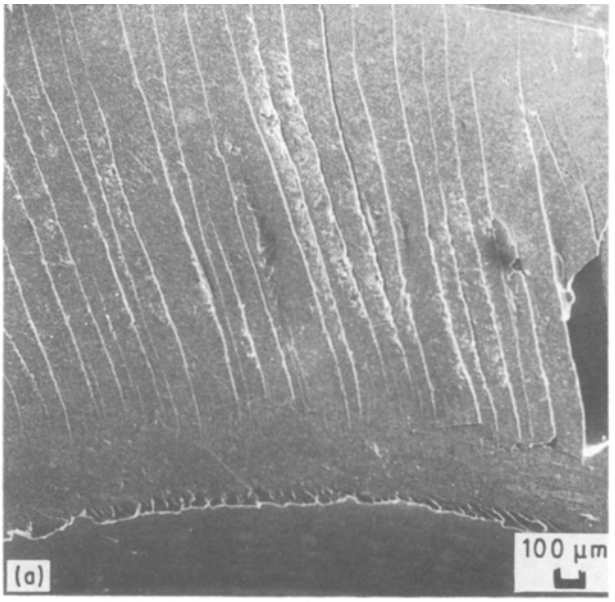

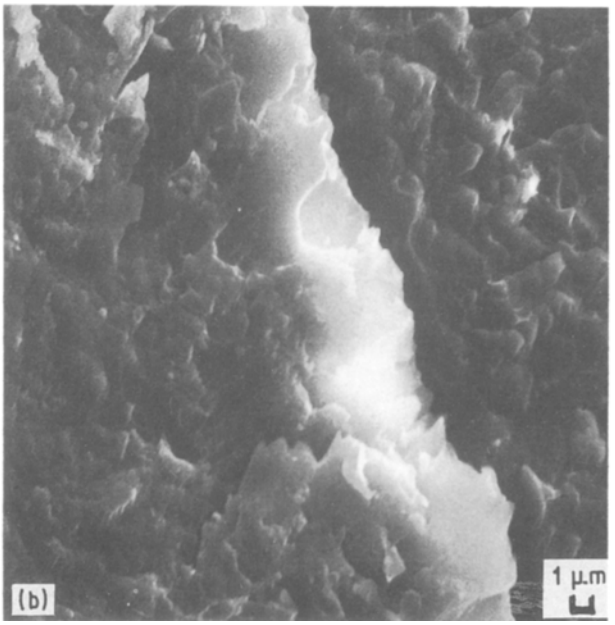

Figure 11 (a, b) As Fig. 10, for $t = 0.11$ mm.

failure occurred at the interface, with no evidence of extensive plastic deformation or distortion within the interlayer. Although the bond has separated at the interface, the failure itself was clearly cohesive; the texture of the adherend surface seems to be fully masked by adhesive. This morphology is much the same as that found in recent mode II fracture tests on adhesive joints made with essentially the same polymeric adhesive as used here [3]. Edge views of the crack-tip region showed that the microcracks traversed the interlayer, making an angle of approximately 45° with the plane of the interface [3]. It was concluded that these microcracks were formed ahead of the crack tip as a result of the tensile stress in the interlayer, which is maximized at the above inclination. More recent tests [19] have vividly demonstrated that crack propagation or bond separation occurs by coalescence of interface microcracks that have extended from the tips of the tensile microcracks.

The micrographs in Figs 12 and 13 represent the morphology for very thin bonds where Δ_f^{nl} increases nearly linearly with t, or, alternatively, γ_f^{nl} is only little affected by t. The morphology for both bonds is characterized by extensive plastic deformation as well as a dense pattern of microcracks. In contrast to Figs 10 and 11, however, the deformation seems to occupy the entire bond thickness. This is particularly evident from the enlarged photo in Fig. 12, where both the lower interface region (upper right corner of the print) and the upper interface (bottom left) can be seen; between these interfaces the material seems highly distorted and cracked.

3.3.2. Toughened epoxy (BP-907)

Figs 14–16 show the morphology for three pivotal bond thicknesses. Similar to its brittle adhesive coun-

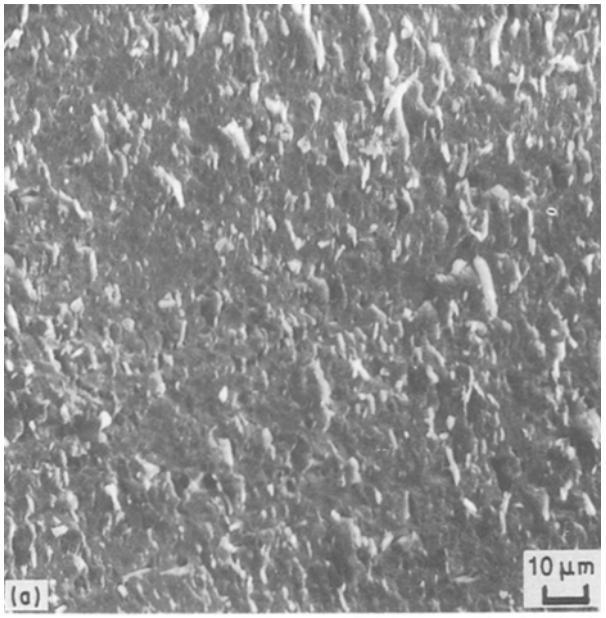

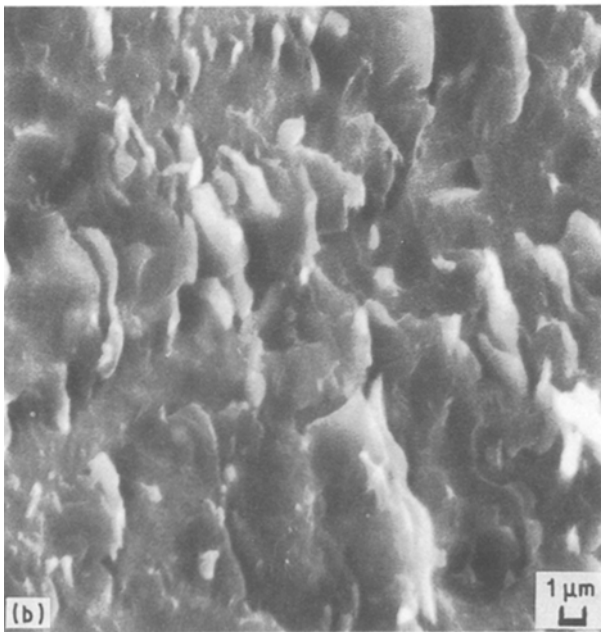

Figure 12 (a, b) As Fig. 10, for $t = 4.3$ μm.

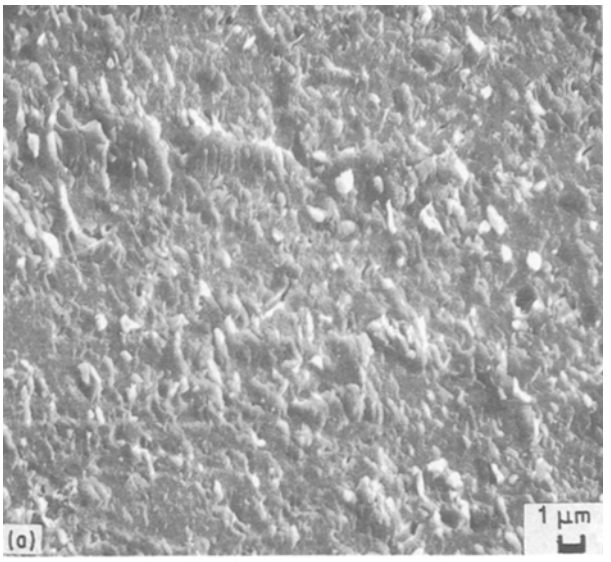

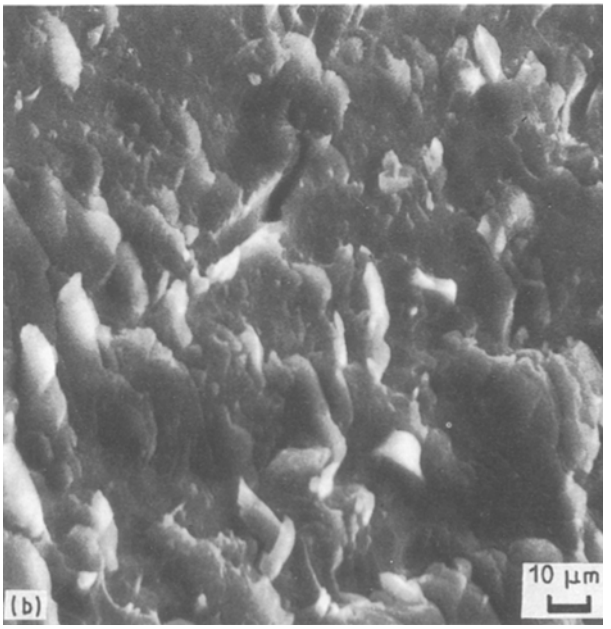

Figure 13 (a, b) As Fig. 10, for $t = 9.4$ μm.

terpart (Figs 12 and 13), the failure of the thin-joint ($t = 5.6$ μm) appears fully cohesive, and it is characterized by extensive plastic deformation and flaws that extend throughout the interlayer. The morphology in Fig. 15 ($t = 15$ μm) characterizes the bond thickness for which the strain–hardening effect is maximized (i.e. $\tau_f/\tau_y = 1.4$). The failure seems to have occurred near the interface, although it is clearly cohesive. The morphology for this bond is distinguished from those of the thin or thick bonds (Figs 14 and 16, respectively), where no strain hardening occurred, by the presence of a lamellar structure whose spatial frequency is a small fraction of a micrometre. It is possible that this texture is due to stretching and orientation of molecular chains or other microstructural entities of the material.

Fig. 16 ($t = 0.285$ mm) corresponds to the same test specimen discussed in Fig. 9. Bond separation is seen to have occurred near the interface, consistent with the discussion of Fig. 9c. Moreover, the sequence of white bands extending generally in the radial direction probably reflect the interaction with the interface of voids such as those shown in Fig. 9. As discussed in that figure, these voids are the precursor to final failure.

4. Discussion

Two possible causes for the variations of adhesive mechanical properties with bond thickness are material changes which may be affected during adhesive cure and variations in the flaw sensitivity of the bond. The former argument can be ruled out considering that the yield stress was independent of bond thickness.

In pursuing the flaw-sensitivity argument, consider a through-the-width Griffith crack of length a in an infinite elastic medium subjected to a remote tensile stress, σ_∞, normal to the crack plane. The plane-strain

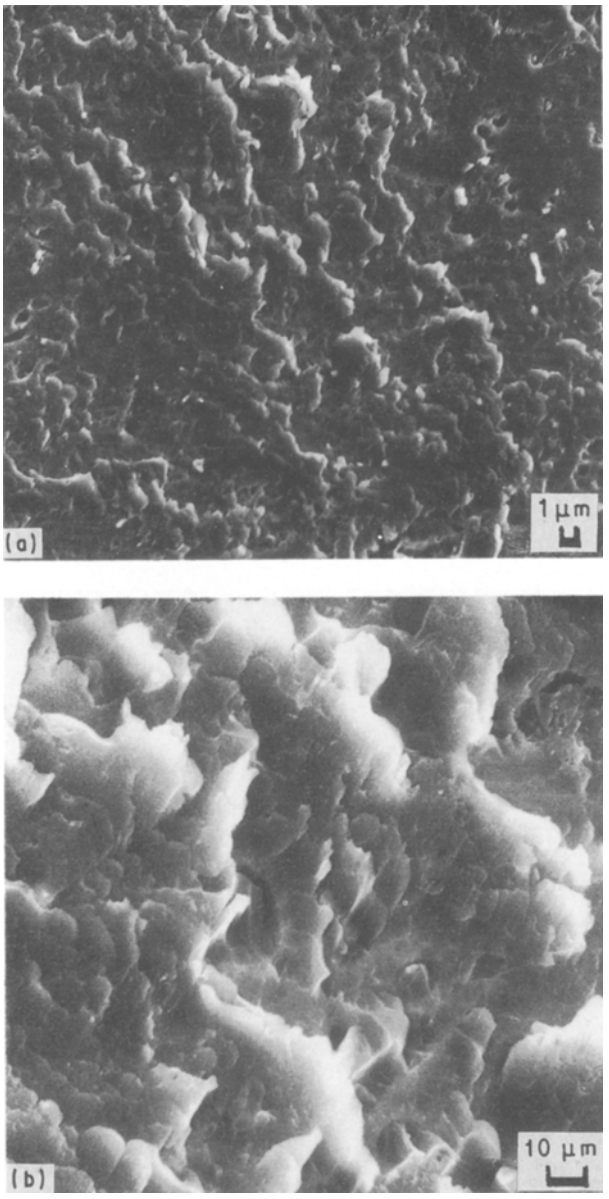

Figure 14 (a, b) Scanning electron micrographs of the failed bond at two magnifications, $t = 5.6$ μm. Adhesive is BP-907.

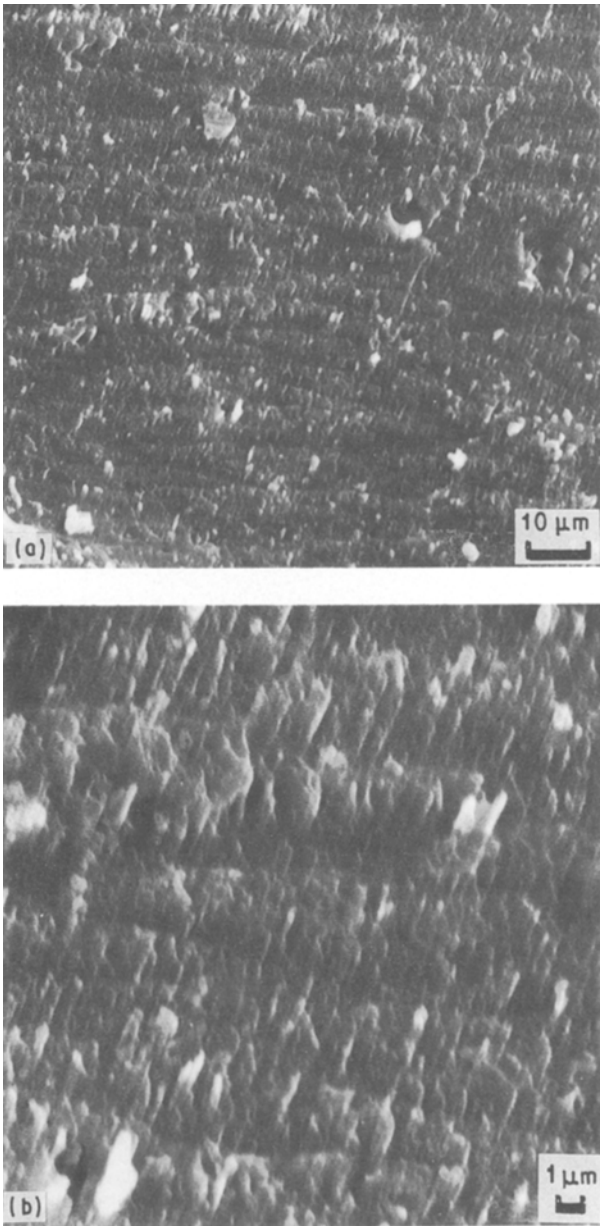

Figure 15 (a, b) As Fig. 14, for $t = 14.7$ μm.

fracture mechanics solution is given by

$$G_I = \frac{(1 - \nu^2)\pi\sigma_\infty^2 a}{2E} \quad (6)$$

where E, ν and G_I are the Young's modulus, Poisson's ratio and the Mode I energy release rate, respectively. It can be easily shown that for the napkin ring specimen, the maximum tensile stress in the adhesive, σ_m, occurs in a plane inclined at 45° to the direction of the applied shear stress. Furthermore, at this inclination, $\sigma_m = \tau$. Neglecting the effect of the adherends, the critical length for microcrack growth, a_{cr}, can be found from Equation 6 by substituting G_{IC} for G_I and τ_y for σ_∞

$$a_{cr} = \frac{2E\,G_{IC}}{(1 - \nu^2)\pi\tau_y^2} \quad (7)$$

Equation 7 may be applied to the brittle adhesive because sharp microcracks oriented at 45° to the shearing direction were indeed present in the bond [3, 19]. Substituting $G_{IC} = 73\ \mathrm{N\,m^{-1}}$ [18], $\tau_y = 110$ MPa (Fig. 3), $E = 4$ GPa and $\nu = 0.33$, one finds $a_{cr} = 17$ μm. The projection of a_{cr} in the thickness direction of the bond is 12 μm. The closeness of this value to the transitional bond thickness in which γ_f^{nl} begins to decline with t (i.e. $t \approx 9$ μm, see Fig. 4) supports the proposition that the latter trend is due to stress concentration effects caused by the microcracks. This seems to be supported also by the SEM results. As discussed earlier, over the bond thickness range where γ_f^{nl} no longer increases with decreasing t (i. e. $t < 9$ μm), intense plastic deformation and microcracking occurred throughout the interlayer, which indicates that the full capacity of the material to deform has been exhausted. Conversely, for $t > 9$ μm, bond separation and extensive plastic deformation were limited to the interface region. This, together with other experimental evidence [19] suggest that a premature failure caused by linkage of adjacent microcracks has preceded the attainment of the ultimate

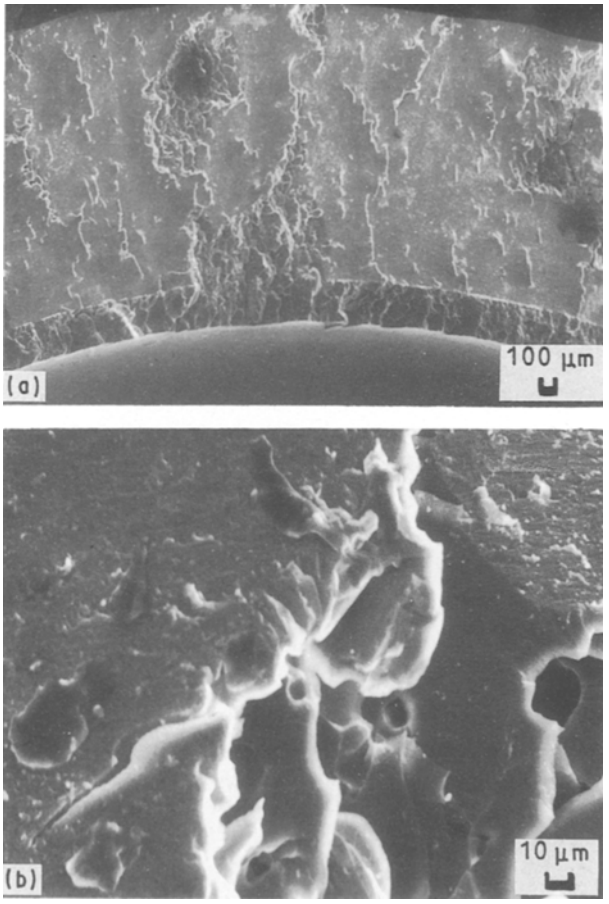

Figure 16 (a, b) As Fig. 14, for $t = 0.285$ mm.

straining capacity of the adhesive. Accordingly, the stabilization of γ_f^{nl} for large values of t may be attributed to a full development of the elastic stresses at the tip of the microcracks. Note that the corresponding value of γ_f^{nl} (10%–15%) is similar to that found when testing the bulk material under special measures to minimize tensile stresses [20].

Unlike for the brittle epoxy, the video records (see Fig. 9) show that for the ductile BP-907 adhesive, the voids have a complex three-dimensional shape so that the applicability of LEFM to predict flaw sensitivity for this material is doubtful. Strength predictions based on void growth models seem more appropriate in this case. Nevertheless, the decrease in γ_f^{nl} with t shown in Fig. 7 is probably due to the development of large strains around voids in thick bonds, the effect that is manifested around Point A in Fig. 9. The greater ultimate shear strain of this adhesive compared to the brittle epoxy evident at large values of t is consistent with the greater fracture resistance found in testing precracked adhesive bonds [19].

Considerable work has been done to elucidate the effect of bond thickness on the tensile and shear strengths of adhesive joints. In both cases, the joint strength is typically found to increase with decreasing t. For tensile loading, this increase is generally attributed to the development of a triaxial state of stress in the adhesive which results from suppression of adhesive necking by the more rigid adherends (see, for example, [18]). For shear loading, the triaxiality argument is less appealing. The improvement in joint strength with decreasing t in this case was attributed to the effect of residual thermal stresses [6] or adhesive straining rate [12]. None of these arguments seems applicable in the present study; for the brittle epoxy, τ_f is essentially independent of t while for the toughened adhesive the increase in joint strength is clearly due to strain hardening. The latter phenomenon occurs also in bulk polymers, e.g. amorphous polycarbonate subjected to shear [21], and it is generally attributed to stretching and orientation of molecular chains [21]. As shown in Fig. 8, this effect occurred only when γ^{nl} exceeds 77%. The results presented indicate that the lack of strain hardening for thick bonds (i.e. $t > 0.165$ mm, see Fig. 6) is due to an early failure caused by void growth. Conversely, the rise in τ_f as t is decreased from 0.04 mm may be attributed to a decrease in the flaw sensitivity of the joint, which allows for a greater material stretching before flaw-induced failure may take place.

The decline in τ_f as t is decreased from approximately 10 μm, common to both adhesives tested, appears somewhat surprising given our earlier argument that the flaw sensitivity diminishes with decreasing t. A possible explanation for this effect is provided by the SEM results. As shown in Figs 12–14, the failure of thin bonds is characterized by extensive microcracking and damage that occupy the entire bond region. This is in contrast to the behaviour for thick bonds where the microcracking density is limited. The denser microcracking damage in thin bonds causes stiffness degradation in the matrix, which may be responsible for the observed trend.

5. Conclusion

The post-yield behaviour of a brittle and a ductile interlayer subjected to shear deformation was studied. The mechanical properties of the adhesive varied with bond thickness. In particular, the ultimate shear strain exceeded 300% when t was decreased to a few micrometres. Experiments and analytical considerations suggest that these variations are controlled by the degree of stress concentration at the tips of tensile microcracks or voids that are formed in the interlayer during the deformation process, not by material changes that may be induced during processing. While the specific dependence of these stress risers on bond thickness has not been elucidated, the limit behaviour for small and large values of t is reasonably well understood. For thick bonds, the stress field around the flaws is fully developed, which leads to the stabilization of γ_f at a small value similar to that of the bulk material. Conversely, for very thin bonds, the driving force at the tip of the microcracks becomes less than the critical value for crack propagation so that the measured ultimate strain most likely represents an intrinsic material property.

For the ductile adhesive, the yield stress was independent of bond thickness. The initial yield was followed by a strain-hardening phase which may be attributed to stretching and orientation of molecular chains. This phase always began when the adhesive

shear strain reached a specific value (77%). For relatively large bond thicknesses, flaw-induced bond failure has preceded the attainment of this critical value, which eliminated the strain-hardening phase. Instead, strain softening occurred once γ^{nc} reached 52%. For both adhesives, the failure stress unexpectedly declined once t was decreased from about 10 μm. SEM analysis showed that this bond thickness regime was distinguished by the occurrence of extensive damage and microcracking that occupied the entire interlayer. The resulting stiffness degradation in the adhesive layer may be responsible for the above trend.

The experiments show that over the bond thickness range used in traditional adhesive bonding applications (i.e. $t > 0.1$ mm), the joint performance is not necessarily the best. The present testing approach offers a reliable means for designing composites, microlaminates and adhesive joints for optimal performance. In current damage tolerance analyses of composites, the properties of the constrained interlayer are generally represented by those of the bulk material. The results presented show that this presumption may be vastly in error. The data also imply that very large displacement gradients may develop within interlaminar resin-rich layers or between adjacent fibres in composite structures loaded beyond the yield point of the matrix. Indeed, this has been demonstrated for unidirectional composite laminates [22, 23]. Unfortunately, current lamination plate theories ignore this effect.

References

1. M. MA, K. VIJAYAN, A. HILTNER and E. BAER, *J. Mater. Sci.* **25** (1990) 2039.
2. S. L. LEHOCZKY, *J. Appl. Phys.* **49** (1978) 5479.
3. H. CHAI, *Int. J. Fract.* **37** (1988) 137.
4. N. A. de BRUYNE, in "Adhesion and Cohesion", edited by P. Weiss (Elsevier, New York, 1962) pp. 47–64.
5. A. BEEVERS, *Mater. Sci. Technol.* **2** (1986) 97.
6. R. W. HYLANDS, in "Adhesive Joints Formation, Characterization and Testing", edited by K. L. Mittal (Plenum Press, New York, 1984) pp. 165–93.
7. V. WEISSBERG and M. ARCAN, in "Adhesively Bonded Joints: Testing, Analysis, and Design", ASTM STP 981, edited by W. S. Johnson (American Society for Testing and Materials, Philadelphia, PA, 1988) pp. 28–38.
8. K. M. LIECHTI and T. HAYASHI, *J. Adhesion* **29** (1989) 167.
9. D. B. CHISHOLM and D. L. JONES, *Exp. Mech.* **17** (1977) 7.
10. L. G. STRINGER, *J. Adhesion* **18** (1985) 185–96.
11. R. F. ZABORA, W. W. CLINTON and J. E. BELL, "Adhesive Property Phenomena and Test Techniques", Air Force Flight Dynamics Laboratory Technical Report AFFDL-TR-71-68, July 1971.
12. R. W. BRYANT and W. A. DUKES, "The Effect of Joint Design and Dimensions on Adhesive Strength", SAE paper 670855, Aeronautic and Space Engineering and Manufacturing Meeting, Los Angeles, CA, 2–6 October, 1967.
13. H. FOULKES, J. SHIELDS and W. C. WAKE, *J. Adhesion* **2** (1970) 254.
14. L. J. HART-SMITH, in "Development in Adhesives-2", edited by A. J. Kinloch (Applied Science, London, 1981) pp. 1–44.
15. RAYMOND B. KRIEGER Jr, in "Proceedings of the 29th National SAMPE Symposium", Anaheim, CA, 3–5 April, 1984, pp. 1570–84.
16. G. W. WYCHERLEY, S. A. MESTAN and IVAN GRABOVAC, *J. Test. Eval.* **18** (1990) 203.
17. JANEL M. MILLER, JANET L. HAMMILL and KENNETH E. LUYK, in "Adhesively Bonded Joints: Testing, Analysis, and Design", ASTM STP 981, edited by W. S. Johnson (American Society for Testing and Materials Philadelphia, PA, 1988) pp. 252–63.
18. H. CHAI, *Engng Fract. Mech.* **24** (1986) 413.
19. *Idem, Int. J. Fract.*, submitted.
20. C. G'SELL, D. JACQUES and J. P. FAVRE, *J. Mater. Sci.* **25** (1990) 2004.
21. C. G'SELL and A. J. GOPEZ, *ibid.* **20** (1985) 3462.
22. J. TIROSH, *J. Appl. Mech.* **40** (1973) 785.
23. D. POST, R. CZARNEK and D. JOH, *Exp. Mech.* **27** (1987) 246.

Received 19 July 1991
and accepted 14 September 1992